APPENDIX A: ANCILLARY DATA

We provide here a brief description of the archival radio and optical images referred to in this paper.

A1 VLA

A1.1 Observations and data reduction

In order to compare the core and jet emission detected at 230 GHz with that visible at lower frequencies, we extracted VLA data at 4.9, 8.5 or 14.9 GHz for our target sources from the NRAO archive. These frequencies were chosen to give a reasonable compromise between high resolution (to match our ALMA images as closely as possible) and sensitivity to extended structure. The datasets are inevitably heterogeneous, with wide ranges of resolution, uv coverage and integration time. In particular, the only data available for NGC 612 have very low spatial resolution. We calibrated the archival data using standard methods, with the flux-density scale set using observations of 3C 48 or 3C 286. Polarization leakage was calibrated for NGC 612 and IC 4296 and the absolute **E**-vector polarization position angle was set for these sources using observations of 3C 286. For NGC 3557, we combined data from three VLA configurations and for NGC 7075 and ESO443−G024 we show images with two combinations of frequency and resolution; in all other cases useful data were only available for a single configuration and frequency. All of the datasets were self-calibrated in phase and amplitude and the final images were made using single or multi-scale CLEAN depending on the complexity of the brightness distribution. The datasets and image parameters are listed in Table A1. We display the linear polarization as vectors with lengths proportional to the degree of polarization, $p = P/I$, where P and I are polarized and total intensity, respectively, orientated along the local **E**-vector direction.

The highest-resolution images available are plotted together with the corresponding 230-GHz images in Figure 1. Lower-resolution images of four sources, ESO443−G024, IC 4296, NGC 612 and NGC 7075, are significantly deeper than any published to date and/or include linear polarization for the first time. These are therefore shown below (Fig. A1 – A3).

A1.2 NGC 612

The image of NGC 612 shown in Figure A1 was made from the same dataset as that analysed by Morganti et al. (1993), but has a significantly lower rms noise level. In addition, linear polarization has been calibrated and the image has been corrected for attenuation by the primary beam. The effects of Faraday rotation on the degree and direction of polarization are 4.9 GHz are very small (Kaczmarek et al. 2018). The apparent magnetic field direction (orthogonal to the plotted vectors) is circumferential in both lobes and transverse in the jets.

A1.3 ESO443−G024 and NGC 7075

The 4.9-GHz images of ESO443-G024 and NGC 7075 (Fig. A2) show the overall structures of the sources, both of which have lobed twin-jet FR I morphologies. The jet structure of ESO443-G024 is symmetrical on large scales (Fig. A2a); side-to-side asymmetry on scales of a few arcseconds is evident from Fig. 1(f), indicating that the NW jet is approaching. For NGC 7075, the base of the NE jet appears brighter even at low resolution (Fig. A2b) and only the NE (approaching) side is visible in the high-resolution VLA and ALMA images (Fig. 1h).

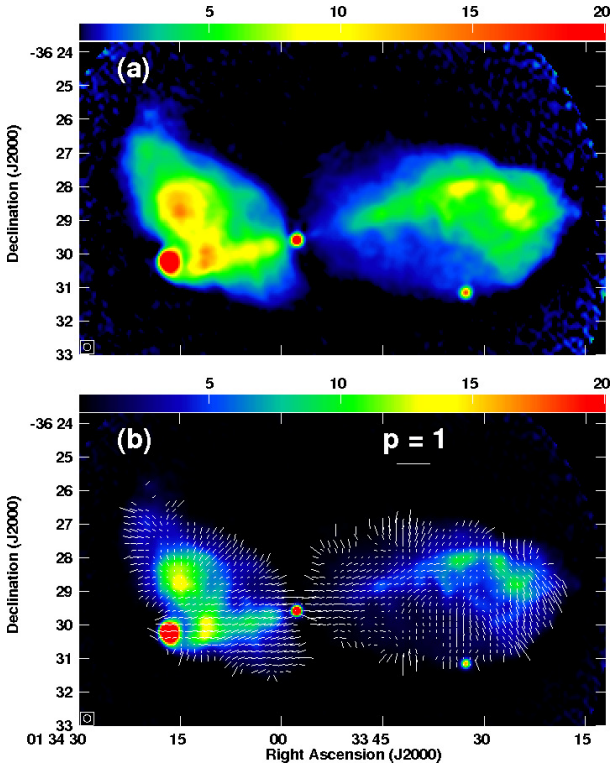

Figure A1. VLA images of NGC 612 at 4.9 GHz. (a) Total intensity in the range 0 – 20 mJy beam^{-1}. The circular pattern visible on the right-hand side of the plot is an artefact caused by the correction for primary-beam attenuation. (b) **E**-vectors with lengths proportional to degree of polarization, $p = P/I$, superimposed on total intensity. The vector scale is indicated by the labelled bar.

A1.4 IC 4296

This source was studied in detail by Killeen et al. (1986), but they did not present images for their highest-resolution 4.9-GHz dataset, which we have therefore re-reduced. The resulting total-intensity images, shown in Fig. A3, have a resolution of 1.58×0.93 arcsec^2 and show the jet bases in detail. The jets are unusually symmetrical and are likely to be close to the plane of the sky. The Faraday rotations estimated for the jets by Killeen et al. (1986) are in the range -40 – 0 rad m^{-2}, implying that the magnitude of the rotation of the observed **E**-vectors from their intrinsic directions is $\lesssim 8°$. The apparent magnetic field within ≈20 arcsec of the core (Fig. A3b) is therefore aligned with the axis on both sides of the nucleus. Figs A3(c) and (d) show polarization vectors for the SE and NW jets, respectively. The magnetic-field structure farther from the core than the flaring points at ≈20 arcsec is remarkably uniform, with an apparent field direction orthogonal to the jet axis and $p \approx 0.3 - 0.5$. IC 4296 and 3C 449 (Feretti et al. 1999) have remarkably symmetrical jet intensity and polarization distributions, consistent with their axes being close to the plane of the sky (e.g. Laing & Bridle 2014).

A2 HST

To investigate the dust-CO connection, we downloaded HST images (available only for NGC 3557 and IC 4296) from the Hubble

Table A1. Archival VLA data used in this study.

Name	Code	Date	t (s)	Config	ν (MHz)	$\Delta\nu$ (MHz)	θ_{maj} (arcsec)	θ_{min} (arcsec)	PA (deg)	RMS (μJy beam^{-1})
(1)	(2)	(3)	(4)	(5)	(6)	(7)	(8)	(9)	(10)	(11)
IC 1531	AH640	1998 06 19	40	A	8460.1	100.0	0.58	0.23	−3.4	210
NGC 612	AK135	1985 10 29	12700	C/D	4860.1	100.0	13.00	13.00	–	29
PKS 0718−34	AL508	1999 10 18	45	A/B	8460.1	100.0	2.29	0.58	14.9	220
NGC 3100	AD270	1991 07 21	260	A	4860.1	100.0	0.90	0.32	−6.9	140
NGC 3557	AB289	1984 12 14	1640	A	4876.1	50.0	1.38	0.35	−12.4	53
	AW136	1985 06 22	340	B/C	4860.1	100.0				
	AB377	1987 02 16	14120	C/D	4860.1	100.0				
ESO443−G024	AJ141	1986 10 04	169	B/C	4860.1	100.0	4.13	3.62	65.9	200
	AM141	1985 02 18	460	A	14938.7	100.0	0.60	0.60	–	970
IC 4296	AE016	1982 07 09	20200	A/B	4872.6	25.0	1.58	0.93	−46.8	55
NGC 7075	AH640	1998 05 18	530	A	8460.1	100.0	0.79	0.22	−2.1	270
	AG478	1996 01 30	35	B/C	4860.1	100.0	5.06	3.59	9.7	110
IC 1459	AG674	2004 09 07	240	A	8460.1	100.0	0.80	0.17	22.2	210

Notes. – Columns: (1) Source name.(2) VLA proposal code. (3) Date of observation. (4) On-source integration time (scaled to 27 antennas). (5) VLA configuration (A/B, B/C and C/D are hybrid configurations with a long N arm).(6) Centre reference frequency. (7) Total bandwidth. (8) Beam major axis. (9) Beam minor axis. (10) Beam position angle. (11) Rms image noise level for I.

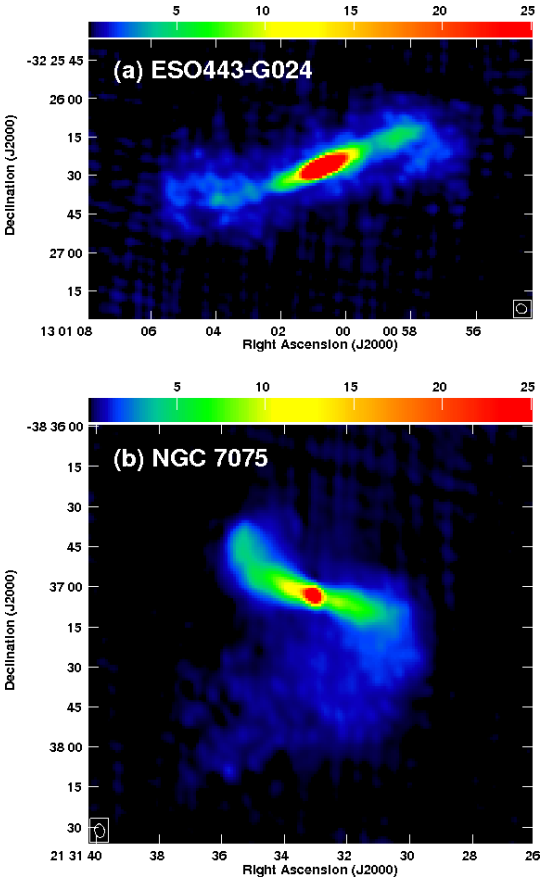

Figure A2. 4.9-GHz VLA images of (a) ESO443-G024 and (b) NGC 7075.

Legacy Archive at the Canadian Astronomy Data Centre (CADC)[1].

This provides enhanced HST image products with an absolute astrometric accuracy ≈0.3 arcsec.

Both galaxies were observed with the HST Wide-Field and Planetary Camera 2 (WFPC2) through the F555W optical filter (λ ≈472−595 nm). The final image products have a pixel scale of 0.1 arcsec pixel^{-1} and an image FWHM of 0.08 arcsec. NGC 3557 was observed on 1997 March 10 with a total on-source time of 1900 s (proposal ID: 6587), IC 4296 on 1997 July 16 with a total exposure time of 1700 s (proposal ID: 6587). Both images are documented by Lauer et al. (2005) and were subsequently used by Balmaverde & Capetti (2006).

The HST images of NGC 3557 and IC 4296 are discussed in Section 6.4 and presented in Figure 11, where they are overlaid on CO integrated intensity maps.

A3 Other optical images

Archival optical images from ground-based telescopes were also available for NGC 612 and NGC 3100 (Fig. 12).

We retrieved the NGC 612 optical image from NED[2]. It was observed with the UK Schmidt Telescope on 1977 September 18 at $\lambda \approx 468$ nm, with a total exposure time of 4500 s. The pixel scale is 1.7 arcsec pixel^{-1}. The B−I image was derived by Véron-Cetty & Véron (2001) from CCD images taken with EFOSC on the ESO 3.6m Telescope.

The optical images of NGC 3100 were retrieved from the Carnegie-Irvine Galaxy Survey (CGS) database[3]. NGC 3100 was observed with the Tek5 CCD camera of the du Pont 2.5-meter telescope at Las Campanas Observatory on 2004 April 19. The observations were made using four filters (Harris B, V, R and I; λ from 300 to 1100 nm). The exposure times were 120 – 360 s in each filter, with resolutions ranging from 0.77 arcsec (B) to 0.62 arcsec (I).

The multi-wavelength set of optical images available for

[1] http://www.cadc-ccda.hia-iha.nrc-cnrc.gc.ca/en/hsthla/

[2] https://ned.ipac.caltech.edu

[3] https://cgs.obs.carnegiescience.edu/CGS/Home.html

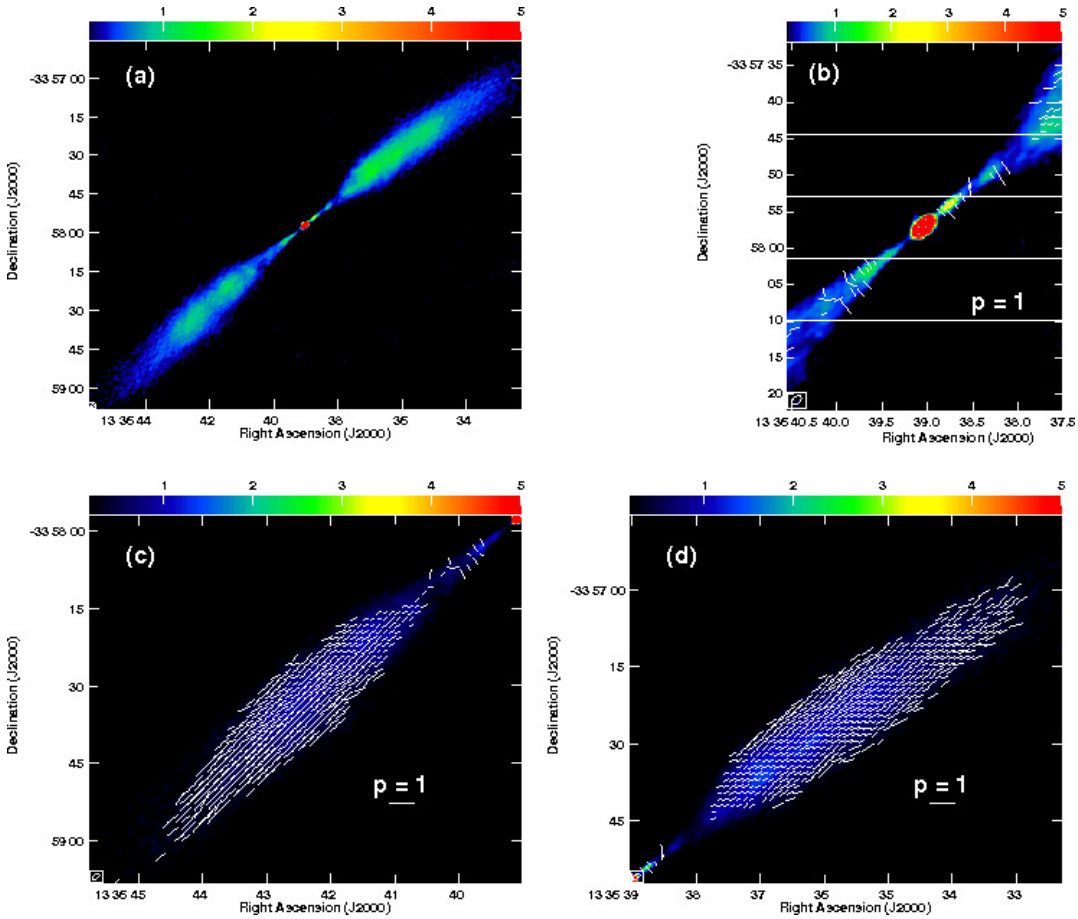

Figure A3. VLA images of IC 4296 at 4.9 GHz. (a) Total intensity. (b) **E**-vectors with lengths proportional to degree of polarization, $p = P/I$, superimposed on total intensity for the inner jets. (c) and (d) As (b), but for larger regions around the SW and NE jets, respectively. The vector scales in panels (b) – (d) are indicated by the labelled bars.

NGC 3100 were used to produce a B-I colour map (bottom-right inset of Fig. 12a). Following de Koff et al. (2000) and de Ruiter et al. (2002), we first scaled the B image (where the dust absorption is most prominent) for the mean magnitude value measured in the I image (where the dust absorption is smallest), and then divided the B by the I image. In the resulting image we assumed that dust absorption features are present where the pixel values are ≤ 0.85 (i.e. where at least 15% of the emission is absorbed). In regions without absorption, the pixel values are close to unity.

REFERENCES

Balmaverde B., Capetti A., 2006, A&A, 447, 97
Feretti L., Perley R., Giovannini G., Andernach H., 1999, A&A, 341, 29
Kaczmarek J. F., Purcell C. R., Gaensler B. M., Sun X., O'Sullivan S. P., McClure-Griffiths N. M., 2018, MNRAS, 476, 1596
Killeen N. E. B., Bicknell G. V., Ekers R. D., 1986, ApJ, 302, 306
Laing R. A., Bridle A. H., 2014, MNRAS, 437, 3405
Lauer T. R., et al., 2005, AJ, 129, 2138
Morganti R., Killeen N. E. B., Tadhunter C. N., 1993, MNRAS, 263, 1023
Véron-Cetty M. P., Véron P., 2001, A&A, 375, 791
de Koff S., et al., 2000, ApJS, 129, 33
de Ruiter H. R., Parma P., Capetti A., Fanti R., Morganti R., 2002, A&A, 396, 857